

Photoswitchable Microgels for Dynamic Macrophage Modulation

Yuri Kim, Ramar Thangam, Jounghyun Yoo, Jeongyun Heo, Jung Yeon Park, Nayeon Kang, Sungkyu Lee, Jiwon Yoon, Kwang Rok Mun, Misun Kang, Sunhong Min, Seong Yeol Kim, Subin Son, Jihwan Kim, Hyunsik Hong, Gunhyu Bae, Kanghyeon Kim, Sanghyeok Lee, Letao Yang, Ja Yeon Lee, Jinjoo Kim, Steve Park, Dong-Hyun Kim, Ki-Bum Lee, Woo Young Jang, Bong Hoon Kim, Ramasamy Paulmurugan, Seung-Woo Cho, Hyun-Cheol Song, Seok Ju Kang, Wujin Sun, Yangzhi Zhu, Junmin Lee, Han-Jun Kim, Ho Seong Jang, Jong Seung Kim, Ali Khademhosseini, Yongju Kim, Sehoon Kim,* and Heemin Kang*

Dynamic manipulation of supramolecular self-assembled structures is achieved irreversibly or under non-physiological conditions, thereby limiting their biomedical, environmental, and catalysis applicability. In this study, microgels composed of azobenzene derivatives stacked via π -cation and π - π interactions are developed that are electrostatically stabilized with Arg-Gly-Asp (RGD)-bearing anionic polymers. Lateral swelling of RGD-bearing microgels occurs via *cis*-azobenzene formation mediated by near-infrared-light-upconverted ultraviolet light, which disrupts intermolecular interactions on the visible-light-absorbing upconversion-nanoparticle-coated materials. Real-time imaging and molecular dynamics simulations demonstrate the deswelling of RGD-bearing microgels via visible-light-mediated *trans*-azobenzene formation. Near-infrared light can induce in situ swelling of RGD-bearing microgels to increase RGD availability and trigger release of loaded interleukin-4, which facilitates the adhesion structure assembly linked with pro-regenerative polarization of host macrophages. In contrast, visible light can induce deswelling of RGD-bearing microgels to decrease RGD availability that suppresses macrophage adhesion that yields pro-inflammatory polarization. These microgels exhibit high stability and non-toxicity. Versatile use of ligands and protein delivery can offer cytocompatible and photoswitchable manipulability of diverse host cells.


1. Introduction

Supramolecular self-assembly has been utilized to create various materials by regulating their intermolecular structures that can determine their nanoscale to macroscale structures and functions.^[1] Supramolecular self-assembly can exhibit 1D,^[2] 2D,^[3,4] and 3D^[1] structures. Inorganic nanoparticles^[5] can also self-assemble to exhibit complex hierarchical^[6] and helical^[7] structures. Moreover, self-assembled materials can encapsulate and release various molecules including macromolecules (such as proteins),^[8] which can add versatility to these materials. Dynamic disassembly of supramolecular self-assembly has been demonstrated under extreme dilution and harsh acidic conditions.^[2] Irreversible but in situ self-assembly has been recently reported in vivo that presents biomedical applicability.^[9] For effective biomedical application of self-assembly, the regulation of immune cell responses, such as macrophage

Yuri Kim, R. Thangam, N. Kang, Sungkyu Lee, S. Min, S. Y. Kim, H. Hong, G. Bae, K. Kim, Sanghyeok Lee, H. Kang
Department of Materials Science and Engineering
Korea University
Seoul 02841, Republic of Korea
E-mail: heeminkang@korea.ac.kr
R. Thangam
Institute for High Technology Materials and Devices
Korea University
Seoul 02841, Republic of Korea

J. Yoo, J. Heo, J. Yoon, Jihwan Kim, S. Kim
Chemical and Biological Integrative Research Center
Korea Institute of Science and Technology
Seoul 02792, Republic of Korea
E-mail: sehoonkim@kist.re.kr

J. Y. Park, Jihwan Kim, Yongju Kim, S. Kim
KU-KIST Graduate School of Converging Science and Technology
Korea University
Seoul 02841, Republic of Korea
K. R. Mun, M. Kang, J. Y. Lee, H. S. Jang
Materials Architecturing Research Center
Korea Institute of Science and Technology
Seoul 02792, Republic of Korea

 The ORCID identification number(s) for the author(s) of this article can be found under <https://doi.org/10.1002/adma.202205498>.

DOI: 10.1002/adma.202205498

phenotype polarization, is crucial. Macrophages display the adhesion-dependent pro-inflammatory (M1) or pro-regenerative (M2) phenotype that dynamically modulate host responses, such as inflammation and tissue regeneration.^[10–17] Robust macrophage adhesion including pronounced assembly of adhesion complexes in an elongated shape is linked with pro-regenerative phenotype.^[18,19] However, switchable self-assemblies in situ via remotely activatable stimuli under physiological aqueous conditions for the regulation of immune cell responses have not been demonstrated, which is a prerequisite for in situ biomedical applications via light-based self-assembly control.

Dynamic materials^[20–29] that can change their structures in response to remotely activatable stimuli,^[30] offer unlimited potential in materials science toward biomedical,^[31] environmental,^[32] energy,^[33] and catalysis^[34] applications. Magnetic fields^[35] readily penetrate materials including human body that can manipulate the movement of magnetically responsive inorganic nanomaterials, such as nanomaterial uncoiling,^[36] nanocluster lifting,^[37] and nanobarcode alignment,^[38] as recently reported by our own studies. However, magnetic fields could neither reversibly change sizes of inorganic magnetic nanomaterials nor be spatially focused for their local manipulation, which necessitates the development of materials that overcomes these limitations.

Light stimulation^[39–41] offers advantages with the capability to be focused and diversity in their wavelength ranges, such as ultraviolet, visible, and near-infrared regions, which can manipulate molecular structures of materials. In particular, ultraviolet light can irreversibly cleave caging molecules to activate RGD-bearing macroscale hydrogels.^[42] Ultraviolet light (U-light) and visible light (V-light) reversibly induce respective *cis*-state and *trans*-state of photoisomers, such as azobenzene currently used for biomedical and energy applications.^[43] Diverse molecules or inorganic nanoparticles have been utilized to demonstrate light-mediated reversible self-assembly, but they all required the use of ultraviolet light^[44–46] with harsh organic solvents^[44,45,47] or several hours of light stimulation^[46] for the switching process to occur. Ultraviolet light is highly tissue-absorptive and toxic that limit their direct use. This can be circumvented by using upconversion nanoparticles (UCNPs)^[48] upconverting near-infrared light to ultraviolet or visible light, which can irreversibly cleave photosensitive molecules to release embedded molecules^[49] or reversibly induce photoisomerization but involves extremely high intensity of near-infrared light (8 W cm⁻²) and thus toxic.^[50,51] Therefore, design of materials that can reversibly change their molecular structures under physiological aqueous conditions without using ultraviolet light can realize

S. Son, J. S. Kim
Department of Chemistry
Korea University
Seoul 02841, Republic of Korea

L. Yang, K.-B. Lee
Department of Chemistry and Chemical Biology
Rutgers University
Piscataway, NJ 08854, USA

Jinjo Kim, Y. Zhu, H.-J. Kim, A. Khademhosseini
Terasaki Institute for Biomedical Innovation
Los Angeles, CA 90024, USA

S. Park
Department of Materials Science and Engineering
Korea Advanced Institute of Science and Technology (KAIST)
Daejeon 34141, Republic of Korea

D.-H. Kim
Department of Radiology
Feinberg School of Medicine
Northwestern University
Chicago, IL 60611, USA

W. Y. Jang
Department of Orthopedic Surgery
Korea University Anam Hospital
Seoul 02841, Republic of Korea

B. H. Kim
Daegu Gyeongbuk Institute of Science and Technology (DGIST)
Department of Robotics and Mechatronics Engineering
Daegu 42988, Republic of Korea

R. Paulmurugan
Department of Radiology
Molecular Imaging Program at Stanford
Stanford University School of Medicine
Stanford University
Palo Alto, CA 94304, USA

R. Paulmurugan
Department of Radiology
Canary Center at Stanford for Cancer Early Detection
Stanford University School of Medicine
Stanford University
Palo Alto, CA 94304, USA

S.-W. Cho
Department of Biotechnology
Yonsei University
Seoul 03722, Republic of Korea

S.-W. Cho
Center for Nanomedicine
Institute for Basic Science (IBS)
Seoul 03722, Republic of Korea

H.-C. Song
Electronic Materials Research Center
Korea Institute of Science and Technology (KIST)
Seoul 02792, Republic of Korea

H.-C. Song
KIST-SKKU Carbon-Neutral Research Center
Sungkyunkwan University (SKKU)
Suwon 16419, Republic of Korea

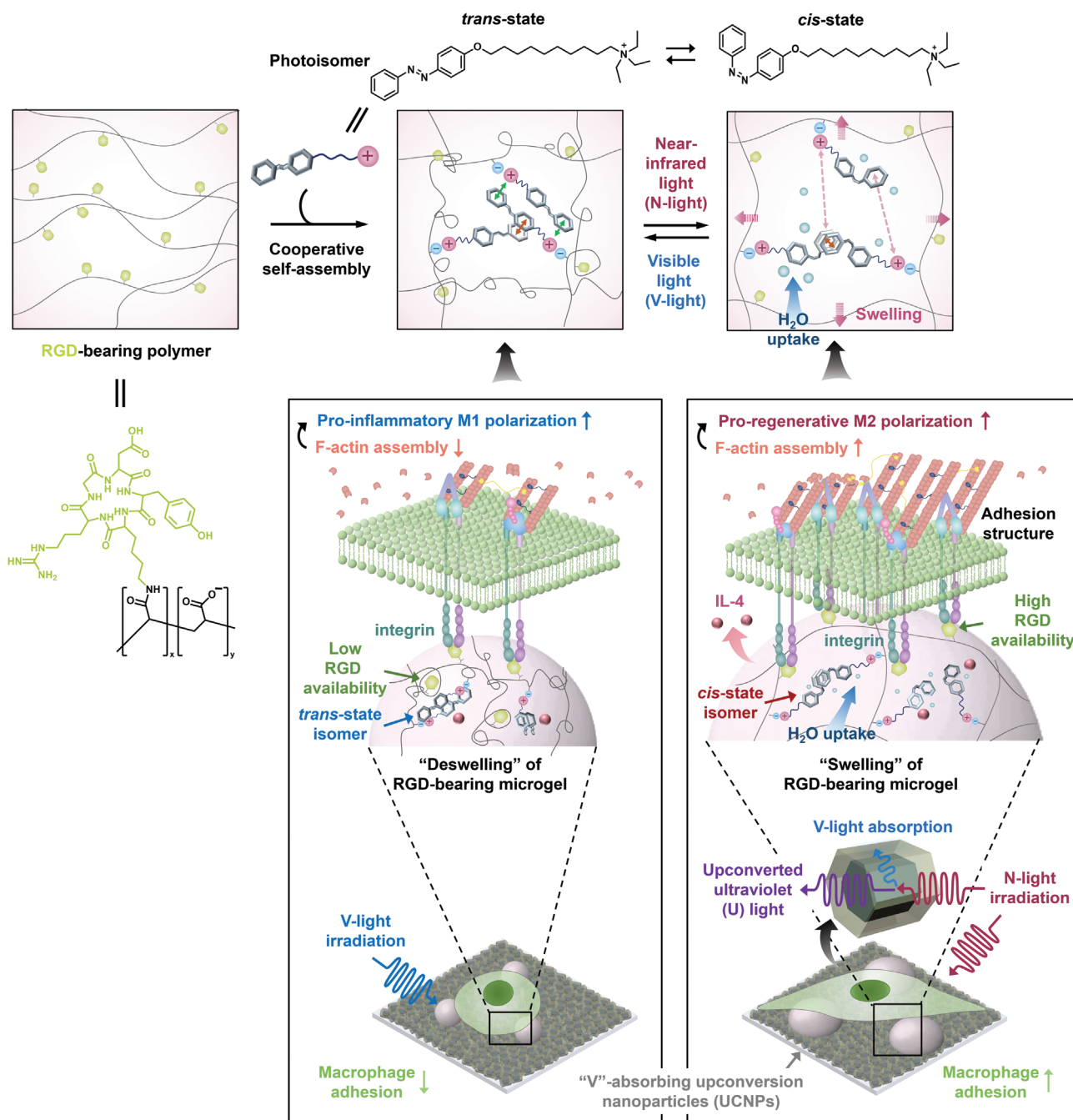
S. J. Kang
School of Energy and Chemical Engineering
Ulsan National Institute of Science and Technology (UNIST)
Ulsan 44919, Republic of Korea

W. Sun
Department of Biological Systems Engineering
Virginia Tech
Blacksburg, VA 24061, USA

J. Lee
Department of Materials Science and Engineering
Pohang University of Science and Technology (POSTECH)
Pohang 37673, Republic of Korea

H. S. Jang
Division of Nano & Information Technology
KIST School
Korea University of Science and Technology (UST)
Seoul 02792, Republic of Korea

H. Kang
College of Medicine
Korea University
Seoul 02841, Republic of Korea



Scheme 1. Schematic summary of the study. The proposed design of mediating cooperative self-assembly of azobenzene derivatives via intermolecular interactions that incorporate RGD-bearing polymers. N-light illumination upconverted to U-light on V-light-absorbing upconversion nanoparticle-coated materials facilitates *cis*-azobenzene formation and thus disrupts intermolecular interactions, which mediates H₂O uptake-mediated lateral swelling of RGD-bearing microgels. V-light illumination mediates *trans*-azobenzene formation and thus enhances intermolecular interactions, which facilitates lateral deswelling of RGD-bearing microgels. N-light illumination triggers IL-4 release from the cell-adhesive RGD-bearing microgels that exhibit swelling-mediated high RGD availability on the V-light-absorbing upconversion nanoparticle-coated materials via N-light-upconverted U-light, thereby stimulating macrophage adhesion linked with pro-regenerative polarization. V-light illumination facilitates deswelling-mediated low RGD availability that suppresses macrophage adhesion that results in pro-inflammatory polarization.

remotely controllable biomedical, environmental, and catalysis applications.

In this study, we demonstrate self-assembled microgels that can exhibit the swelling and deswelling in five cycles via

near-infrared light (N-light) and V-light irradiation without using U-light using the UCNPs and V-light-absorbing natural dyes for preferential N-light-to-U-light conversion (Scheme 1). Microgels are formed by stacking azobenzene derivatives

(Azo-C₁₀-N⁺ molecules) via π -cation and π - π interactions that electrostatically incorporate RGD-bearing polymers. We utilize UCNP_s to induce *cis*-azobenzene formation, which disrupts π -cation interactions in twisted structures, thereby increasing polarity and hydrophilicity as well as mediating swelling of RGD-bearing microgels via H₂O uptake to trigger loaded interleukin-4 (IL-4) release. *Trans*-azobenzene formation induced by V-light increases π -cation interactions and hydrophobicity as well as mediating deswelling of RGD-bearing microgels.

The switching between the lateral swelling and deswelling of RGD-bearing microgels via irradiation of N- and V-light enables a system to remotely control positional changes in RGDs according to the lateral swelling and deswelling of the RGD-bearing microgels that can dynamically regulate macrophages. Owing to their photoswitching capability in physiological aqueous solution, remotely controllable stimuli enable N-light-mediated swelling that yields high RGD availability. This stimulates macrophage adhesion structure formation^[52] that mediates pro-regenerative polarization. In stark contrast, V-light-mediated deswelling that yields low RGD availability suppresses macrophage adhesion, resulting in pro-inflammatory polarization. We present the switchable microgels offering high RGD availability under physiological conditions, which can be used for diverse potential applications. Our system can offer versatile applications not only for biomedical therapy and diagnosis, but also for environmental purifications, catalysis,^[32] solar cells, batteries, and electronics.^[53] Our system can be used for in situ biomedical applications, including the regulation of host immune cell responses, including such as macrophages, neutrophils, and monocytes, and protein delivery.^[54,55] Upon photoisomerization-regulated swelling and deswelling, microgels can uptake and extract body fluids for diagnosis applications. Also, our light-controllable system can also be utilized as solar thermal fuels that can capture and convert solar energy into thermal energy and release the energy via photoisomerization.

2. Results and Discussion

2.1. Light-Controlled Swelling and Deswelling of RGD-Bearing Microgels

Azo-C₁₀-N⁺ molecules were synthesized to mediate the self-assembly of microgels (Figure S1, Supporting Information). Azo-OH was first synthesized by mixing 4-aminophenol and nitrosobenzene in acetic acid. Then, 1,10-dibromodecane was conjugated to the Azo-OH to obtain Azo-C₁₀-Br by mixing Azo-OH and 1,10-dibromodecane in dimethylformamide with sodium hydride. Finally, Br in the Azo-C₁₀-Br molecules was replaced by triethylamine via mixing Azo-C₁₀-Br and triethylamine in acetonitrile to obtain the Azo-C₁₀-N⁺ product. ¹H NMR spectra of Azo-OH, Azo-C₁₀-Br, and Azo-C₁₀-N⁺ molecules exhibit characteristic peaks of phenolic group at 10.34 ppm, ether group at 4.05 ppm, and α -hydrogens to tertiary amine at 3.54–3.25 ppm, respectively, thereby confirming successful synthesis of the Azo-C₁₀-N⁺ molecules (Figure S2, Supporting Information). To incorporate RGDs in the microgels, RGD-anchored negatively charged polymers [poly(acrylic acid) (PAA)] were synthesized and then incorporated in the microgels of

stacked Azo-C₁₀-N⁺ molecules via electrostatic interactions. The amine group-bearing lysine residue of the cyclo-RGDyK was coupled to the carboxylate group of PAA (*M_w* = 1800 Da) (Figure S3, Supporting Information).

The microgels can be mediated by facilitating the stacking of Azo-C₁₀-N⁺ molecules via intermolecular interactions while simultaneously incorporating negatively charged RGD-bearing PAA (Figure S4, Supporting Information). Molecular dynamics (MD) simulations were employed to examine the effect of switching between the *trans*- and *cis*-states of the Azo-C₁₀-N⁺ molecules on the degree of their stacking via intermolecular interaction mechanism and H₂O uptake in the microgels by modifying our previous conditions.^[4] Representative snapshots of MD simulations of Azo-C₁₀-N⁺ molecules in *trans*- and *cis*-state revealed that intermolecular π interactions of the Azo-C₁₀-N⁺ molecules were facilitated in *trans*-state with incorporation of N⁺ cation and the spacer of hydrophobic tail, which mediated the stacking of the Azo-C₁₀-N⁺ molecules (Figure S5a, Supporting Information). A heat map chart and frequency counts of the π -cation interactions of the Azo-C₁₀-N⁺ molecules at 20 ns of the MD simulations further confirmed that these interactions were significantly facilitated in the *trans*-state of Azo-C₁₀-N⁺ molecules than the *cis*-state, while the degree of π - π interactions was similar in both states (Figure 1a,b; Figure S5b,c, Supporting Information). Density functional theory (DFT) calculations revealed that the Azo-C₁₀-N⁺ molecules in the *cis*-state exhibited considerably higher hydration energy and larger polar surface area, thereby indicating markedly higher H₂O affinity than those in the *trans*-state (Figure S5d,e, Supporting Information). Taken together, we suggest that enhanced polarity and hydrophilicity of the twisted structure of *cis*-Azo-C₁₀-N⁺ molecules with suppressed π -cation interactions facilitate the H₂O uptake-mediated swelling of RGD-bearing microgels. In stark contrast, π -cation interactions in relatively non-polar *trans*-Azo-C₁₀-N⁺ molecules mediate their dense microgels that restrain the H₂O uptake-assisted swelling of RGD-bearing microgels.

We next conducted MD simulations using two Azo-C₁₀-N⁺ molecules in the *trans*- or *cis*-state with acrylic acid, which confirmed that acrylic acid remained associated with self-assembled Azo-C₁₀-N⁺ molecules in both *trans*- and *cis*-states (Figure 1c). UV-vis spectroscopy was conducted for the reference of “relative degree of *trans*-to-*cis* isomerization” revealing the wavelength of peak intensities to be 345 nm after V-light treatment (indicating maximum degree of *trans*-state formation) and 315 nm after U-light treatment at 0 h (indicating maximum degree of *cis*-state formation), which was nearly maintained for 24 h with minimal peak shifts (Figure 1d,e). Azo-C₁₀-N⁺-assembled microgels exist in a photostationary state in which the *cis*- and *trans*-state dominate following U- and V-light irradiation, respectively.^[56,57] We confirmed through UV-vis absorbance that the microgels reach the photostationary state following U- or V-light irradiation (Figure 1d). Time-dependent relative degree of *trans*-to-*cis* isomerization after U-light treatment was derived based on its absorbance at 375 nm,^[56,58] where 100% means U-light photostationary state (in the maximum degree of the *cis*-state) and 0% means V-light photostationary state (in the maximum degree of the *trans*-state), which were used as standard boundary. Quantification

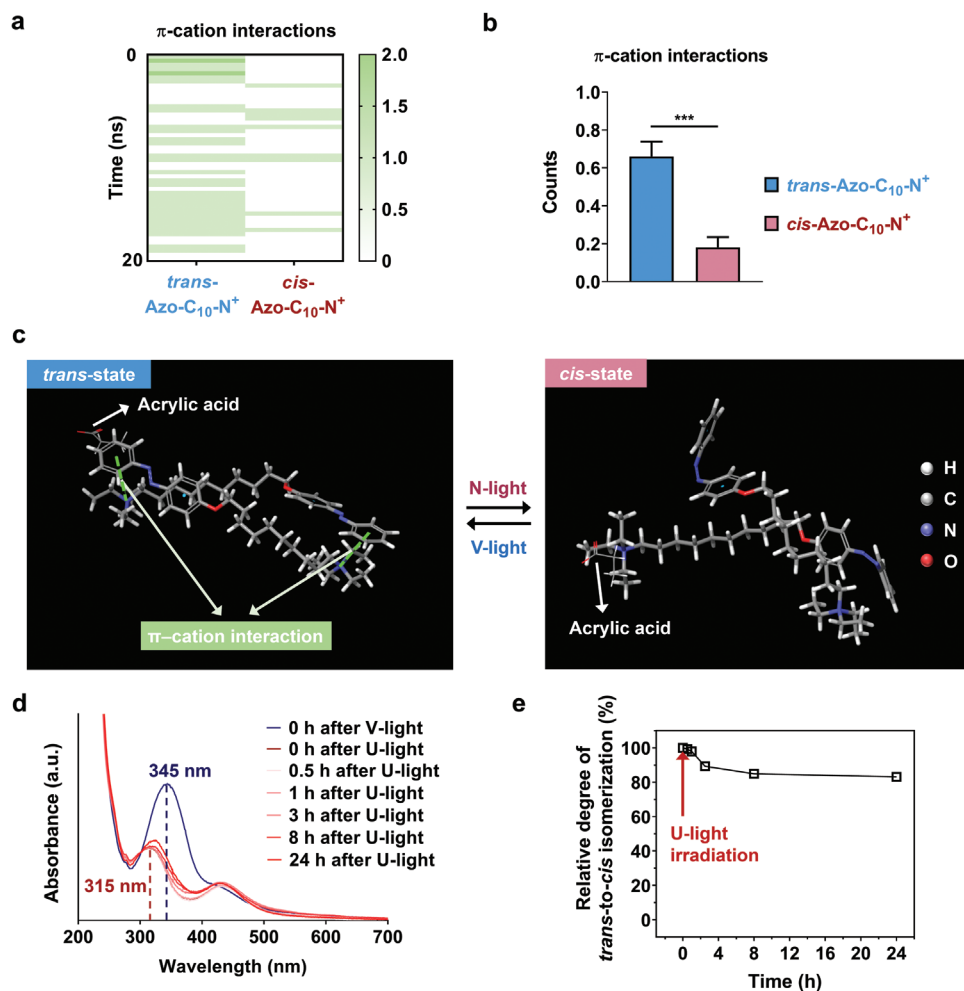


Figure 1. Light-mediated cyclic switching facilitates the swelling of microgels via *cis*-Azo-C₁₀-N⁺ state disrupting intermolecular interactions. a) Molecular dynamics (MD) simulations of a heat map chart and b) frequency counts of π -cation interactions in the *trans*- or *cis*-state Azo-C₁₀-N⁺ molecules at 20 ns in the MD simulation, as well as c) representative snapshots of *trans*- and *cis*-state Azo-C₁₀-N⁺ molecule with acrylic acid. d) Time-dependent changes in the UV-vis absorption spectra after initial V-light (448 nm at 0.2 W cm⁻²) treatment for 30 s and subsequent U-light (365 nm at 0.25 W cm⁻²) treatment for 30 s with dotted lines drawn at 315 and 345 nm, which indicate wavelengths of absorption peak of maximum relative degree of the *cis*- and *trans*-Azo-C₁₀-N⁺ in the microgels, respectively. e) Corresponding relative degree of *trans*-to-*cis* isomerization of Azo-C₁₀-N⁺ in the microgels shown as percentage (%) determined using relative absorbance values at 375 nm at various time points. Data are shown as the mean \pm standard error ($n = 3$). Asterisks were assigned to p values with statistically significant significances (***: $p < 0.001$).

of the time-dependent relative degree of *trans*-to-*cis* isomerization after U-light treatment confirmed that its percentage was >80% after 24 h, indicating that it is stable for day-scale after U-light treatment for 30 s (Figure 1e). This long lifetime of *cis*-state is in accordance with the design of the azobenzene derivative that exhibits relatively blue-shifted absorbance peak in the *trans*-state.^[43] The UV-vis absorption spectra and time-dependent relative degree of *trans*-to-*cis* isomerization over 5 cycles of U-light treatment for 30 s following V-light treatment for 30 s confirm that the switching between the maximum *cis*-state and *trans*-state was nearly 100% for 5 cycles (Figure S6a–l, Supporting Information). Additionally, we estimated critical aggregate concentration of the formation of microgels via dynamic light scattering (DLS) analysis, which was estimated to be 0.66 mg mL⁻¹ (Figure S7, Supporting information). During all of our experiments, we used precursor concentration

of 5.12 mg mL⁻¹, which is above critical aggregation concentration to consistently yield the microgels.

2.2. N-Light-Upconverted U-Light- and V-Light-Regulated Swelling of RGD-Bearing Microgels

To remotely control the swelling and deswelling of RGD-bearing microgels via tissue-penetrative stimuli without using U-light, we synthesized UCNPs that upconvert N-light to U-light. UCNP (C), UCNP (C@S), and UCNP (C@S@D) refer to core UCNP, core@shell UCNP, and core@shell@dye UCNP, respectively. UCNPs were designed as core@shell nanostructures (NaYF₄:Yb,Tm@NaYF₄) through the epitaxial growth of the UCNP shell on the UCNP (C) to obtain the UCNPs free of surface defects, which enhances N-light-excited photoluminescence

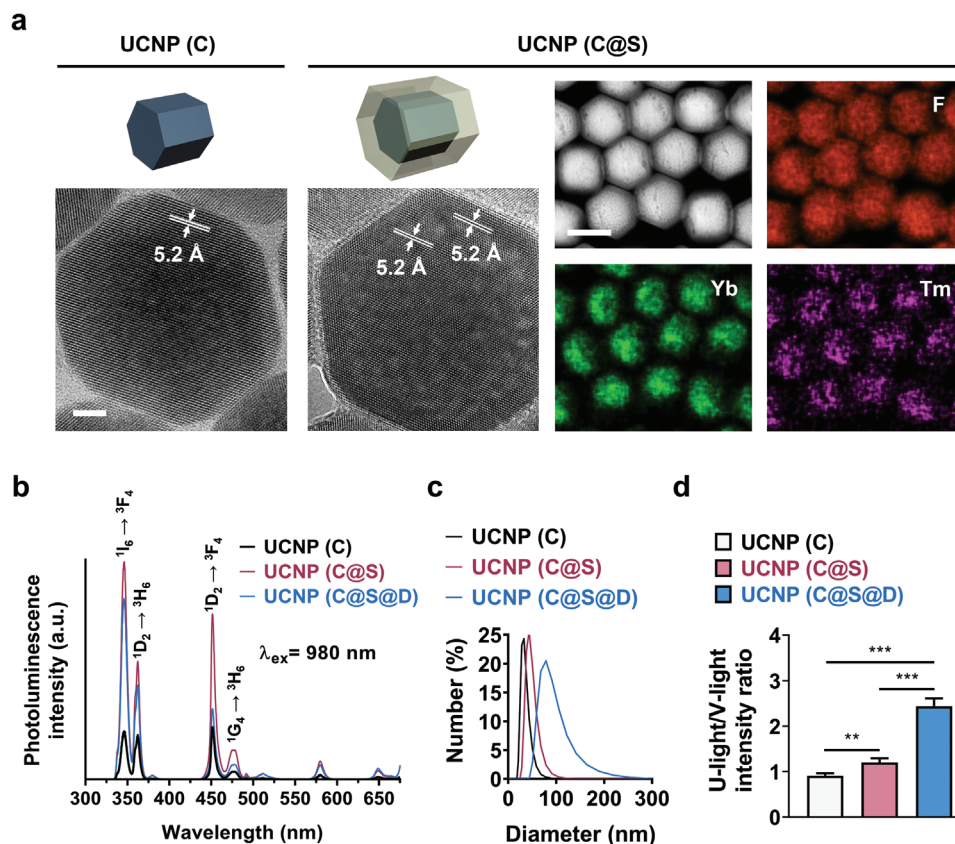


Figure 2. UCNP (C@S@D) exhibits significantly enhanced photoluminescence intensity and preferential upconversion of N-light to U-light. a) Schematic and high resolution-transmission electron microscopy (HR-TEM) images of the UCNP (C) and UCNP (C@S) in atomic scale. An average lattice spacing of 5.2 Å corresponding to the (1010) crystalline plane in hexagonal phase was assigned to neighboring periodic lattice fringes in the core and epitaxially grown shell regions. High-angle annular dark-field scanning TEM (HAADF-STEM) and energy-dispersive X-ray spectroscopy (EDS) mapping of the UCNP (C@S). In the EDS mapping, F element is present in both the core and shell of the UCNPs while Yb and Tm elements are only present in the UCNP (C). b) Photoluminescence spectra of the UCNP (C), UCNP (C@S) and UCNP (C@S@D) under N-light (980 nm) excitation. Each peak is labeled according to the orbital shell transition responsible for producing photoluminescence. c) Dynamic light scattering (DLS) to measure the diameter of the UCNP (C), UCNP (C), and UCNP (C@S@D). d) U-light/V-light intensity ratio of the UCNP (C), UCNP (C@S), and UCNP (C@S@D) under N-light (980 nm) excitation. The U-light/V-light intensity ratio was calculated by dividing the maximum peak intensity in the U-light (340 nm) region by that in the V-light (450 nm) region. Scale bars: 5 nm (HR-TEM) and 50 nm (HAADF-STEM and EDS mapping). Data are shown as the mean \pm standard error ($n = 6$). Asterisks were assigned to p values with statistically significant significances (**: $p < 0.01$; ***: $p < 0.001$).

intensity.^[48,59] The transmission electron microscopy (TEM) and high resolution-TEM (HR-TEM) images confirmed homogeneous size distribution and morphology of the synthesized UCNP (C) and UCNP (C@S) (Figure 2a; Figure S8, Supporting Information). The HR-TEM images revealed that lattice fringes of the UCNP (C) and UCNP (C@S) confirm the hexagonal crystalline structure of both the core and shell part of the UCNP. High-angle annular dark-field scanning transmission electron microscopy (HAADF-STEM) and energy-dispersive X-ray spectroscopy (EDS) mapping of the UCNP (C@S) revealed the distributions of F and Y elements in both the core and shell structures, as well as the Yb and Tm dopant elements present in the core structure (Figure 2a; Figure S8, Supporting Information).

The synthesized UCNP (C) exhibited photoluminescence peaks in both the U-light and V-light (blue) regions under N-light (980 nm) excitation (Figure 2b). These U-light peaks were originated from electronic transitions of $^1I_6 \rightarrow ^3F_4$ and $^1D_2 \rightarrow ^3H_6$ in Tm^{3+} and the blue peaks were attributed to

$^1D_2 \rightarrow ^3F_4$ and $^1G_4 \rightarrow ^3H_6$ transitions in Tm^{3+} . When UCNP shell was epitaxially grown on the UCNP (C) to passivate surface defects, the photoluminescence intensity of the resulting UCNP (C@S) was markedly increased compared to the UCNP (C) alone (Figure 2b). DLS analysis showed an increase in the homogeneously distributed hydrodynamic diameter of 34 \pm 0.9 nm in the UCNP (C) to 47 \pm 1.2 nm in the UCNP (C@S) (Figure 2c). To selectively induce *cis*-Azo- C_{10} - N^+ formation that mediates the swelling of RGD-bearing microgels by N-light-converted-U-light, the transduction of N-light to U-light over N-light to V-light was maximized by using clinically used natural dye (β -carotene)^[60] that absorbs V-light, particularly in the blue region with wavelength from 400 to 500 nm (Figure S9a, Supporting Information). On the other hand, *trans*-Azo- C_{10} - N^+ formation can be induced by V-light to deswell RGD-bearing microgels. Therefore, N-light must be preferentially converted to U-light over V-light to specifically induce *cis*-Azo- C_{10} - N^+ formation. To this end, the UCNP (C@S) was coated with this V-light-absorbing dye to yield the

UCNP (C@S@D), which showed the hydrodynamic diameter of 89 ± 3.1 nm (Figure 2c).

N (980 nm)-excited photoluminescence spectra and calculated U-light (340 nm) to V-light (450 nm) photoluminescence intensity ratio revealed that U-light/V-light intensity ratio gradually increased from the UCNP (C), to the UCNP (C@S), and to the UCNP (C@S@D) although the PL intensity of the UCNP (C@S@D) slightly decreased compared to that of UCNP (C@S) (Figure 2b,d). This U-light/V-light intensity ratio supported relatively preferential upconversion of N-light to U-light over N-light to V-light that evidently occurred in the UCNP (C@S@D) (Figure 2d). The photographs of the N-light-excited photoluminescence consistently confirmed high-intensity blue photoluminescence in the UCNP (C@S), which decreased in the UCNP (C@S@D) (Figure S9b, Supporting Information). The substrate surface was fully covered with the UCNP (C@S@D) (Figure S9c, Supporting Information). The U-light/V-light intensity ratio was significantly increased from the UCNP (C@S)-coated substrate to the UCNP (C@S@D)-coated substrate under N-light (980 nm) excitation (Figure S9d,e, Supporting Information). Therefore, we used the UCNP (C@S@D)-coated substrate throughout this study since it exhibits preferential upconversion of N-light to U-light in high intensity.

The RGD-bearing microgels were attached to the UCNP (C@S@D)-coated substrate via hydrophilic interactions between the RGD-bearing microgels and the surface of the UCNP (C@S@D) on a substrate. This ensured that the UCNPs, dyes, and Azo- C_{10} - N^+ molecule-containing RGD-bearing microgels were in close contact with one another, which facilitated efficient control over the swelling of RGD-bearing microgels by N-light-upconverted U-light via *cis*-state formation of the Azo- C_{10} - N^+ molecules. All contact angles of a water droplet on the UCNP (C@S@D)-coated silicon substrate and glass substrate with and without microgels were $<10^\circ$ that confirm the existence of hydrophilic interactions (Figure S10a,b, Supporting Information). The deswelling of RGD-bearing microgels was facilitated by direct illumination of V-light to produce *trans*-state formation of the Azo- C_{10} - N^+ molecules. The RGD-bearing microgels were attached to the UCNP (C@S@D) surface via intermolecular interactions to allow repeated switching of swelling and deswelling of RGD-bearing microgels on the UCNP (C@S@D)-coated substrate.

To explore capability of RGD-bearing microgels to encapsulate molecules, we examined the loading of rhodamine into the RGD-bearing microgels. During loading rhodamine into the microgels, Azo- C_{10} - N^+ molecules and PAA may physically entrap rhodamine during the formation of microgel network (Figure 3a). The number of RGD-bearing microgels per unit area was 4990 ± 233 microgels mm^{-2} . We next conducted light-mediated swelling and deswelling of RGD-bearing microgels. The number of RGDs per microgels was nearly constant in the swelling ($2.23 \pm 0.11 \times 10^{10}$) and deswelling ($2.03 \pm 0.03 \times 10^{10}$) states of RGD-bearing microgels (Figure 3b). The fully saturated wet weight divided by the dry weight of RGD-bearing microgels in the light-mediated swelling state was markedly increased by 308% due to H_2O uptake compared to that of the light-mediated deswelling state (Figure 3b). Therefore, we speculate that the swelling and deswelling of the RGD-bearing

microgels modulate the degree of RGD availability (rather than the number of RGDs) and the RGDs available in the microgels are thus saturated in similar numbers in those two states. Swelling promotes H_2O intake into the sparsely stacked structure of the Azo- C_{10} - N^+ molecules that facilitates uncoiling of the RGD-bearing polymers, thereby yielding high RGD availability. In stark contrast, deswelling inhibits H_2O intake into the densely stacked structure of the Azo- C_{10} - N^+ molecules that causes coiling of the RGD-bearing polymers, thereby offering low RGD availability.

DLS analysis of microgels was conducted to quantitatively evaluate the change in hydrodynamic diameter of microgels in the pre-treatment, swelling, and deswelling state, which confirmed the diameter was significantly higher in swelling state than in the pre-treatment and deswelling state (Figure S11, Supporting Information). Fluorescence imaging and quantification of red-fluorescent rhodamine-loaded microgels revealed there is no significant difference in the average diameter of the microgel in the pre-treatment (2.51 ± 0.61 μm) and deswelling state (2.45 ± 0.40 μm) (Figure 3c,d). In contrast, there was significant difference when comparing microgel in the pre-treatment and deswelling state with the swelling state (3.84 ± 1.29 μm). Furthermore, we conducted in situ bright-field imaging on the same area to confirm the light-mediated in situ swelling and deswelling of RGD-bearing microgels. We found that the RGD-bearing microgels exhibited in situ swelling under U-light for 1 min and in situ deswelling under V-light for 9 min (Figure S12 and Movie S1, Supporting Information). The time-lapse snapshot images revealed that the RGD-bearing microgels stay focused on the same plane during in situ swelling and deswelling, thereby confirming their lateral swelling and deswelling while minimizing their axial changes.

According to the swelling and deswelling of RGD-bearing microgels, both the diameter and percentage of total lateral area of the RGD-bearing microgels were increased and decreased with significant differences, respectively (Figure 3c,d; Movie S1, Supporting Information). Thus, the percentage of the total lateral area of RGD-bearing microgels (calculated by multiplying the number of RGD-bearing microgels per unit area by the lateral section area of each microgel) was found to significantly increase in the swelling state as compared to the deswelling state (Figure 3b). We found that the percentage of the total lateral area of RGD-bearing microgels was comparable to that of the RGD-bearing gold nanoparticles that were shown to efficiently regulate cell adhesion in previous studies,^[61,62] indicating that the RGD density used in our current study could sensitively regulate cell adhesion in a time-resolved manner via the swelling and deswelling of RGD-bearing microgels. Our present study is differentiated from previous studies that have shown dynamic manipulation of supramolecular self-assembled structures via irreversible in situ self-assembly^[9] or reversible but extreme dilution and harsh acidic conditions.^[2]

2.3. Light-Controlled Temporal Macrophage Adhesion

As a model of applications of remotely controllable system, we investigated whether positional changes in the RGDs occurring in the swelling and deswelling of RGD-bearing

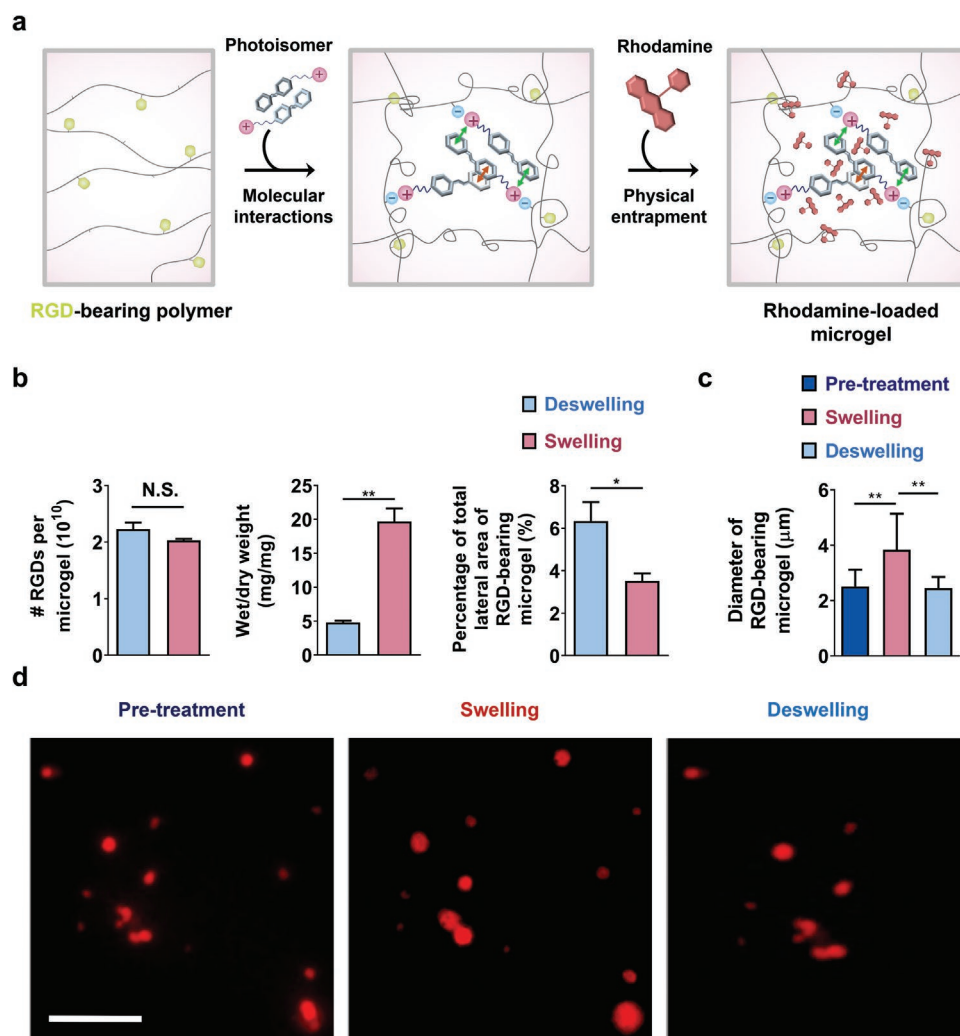


Figure 3. Light-mediated swelling of RGD-bearing microgels. a) A schematic of the loading of red-fluorescent rhodamine into the RGD-bearing microgels. b) Quantifications of the number of RGDs per microgel, the swelling ratio (the ratio of the wet weight to the dry weight of the microgels), and the percentage of the total lateral area of RGD-bearing microgels in swelling and deswelling state on the substrate facilitated by U-light (365 nm, 0.25 W cm^{-2}) and V-light (448 nm, 0.2 W cm^{-2}) irradiation, respectively. c) Quantification of the diameter and d) fluorescent images of rhodamine-loaded RGD-bearing microgels in the pre-treatment, swelling, and deswelling state. Scale bars: $10 \mu\text{m}$. Data are presented as the mean \pm standard error ($n = 3$ for b and $n = 10$ for c). Asterisks were assigned to p values with statistically significant significances (*: $p < 0.05$; **: $p < 0.01$). N.S. signifies non-statistically significant differences.

microgels via N- and V-light irradiation, respectively, can dynamically regulate macrophage adhesion (Scheme 1). This is due to unique characteristics of our material system that can reversibly change their molecular structures in physiological aqueous solution without using U-light, thus suitable for biomedical applications. We used glass and silicon substrates for in vitro and in vivo experiments, respectively, and found that temperature changes of these substrates (microgels on the UCNP (C@S@D)-coated substrate) before and after N- or V-light irradiation lied within $3 \text{ }^\circ\text{C}$, which would not cause any damage to the cells and tissues (Figure S13a,d, Supporting Information).

Macrophages exhibit comparable size to that of our RGD-bearing microgels ($3\text{--}5 \mu\text{m}$) that can help to examine direct correlation between macrophage and RGD-bearing microgels. Thus, we plated macrophages only at 0 h and

explored the light-mediated control of macrophage adhesion on the RGD-bearing microgels attached to the UCNP (C@S@D)-coated substrate that enables the transduction of N- to U-light. We irradiated N-light (980 nm) at an intensity of 1 W cm^{-2} for 1 min or V-light (448 nm) at an intensity of 0.2 W cm^{-2} for 10 min at 0 and 12 h and compared the macrophage responses after 24 h to control group without light irradiation (“No light”). We found that macrophages readily adhered onto the RGD-bearing microgels in swelling state that offer high RGD availability and exhibited pronounced assembly of integrin $\beta 1$, F-actin filaments, and focal adhesion kinase (FAK) with elongated shape via confocal immunofluorescence imaging of the “N-light” group (Figure S14a, Supporting Information). In contrast, macrophage adhesion was neither prominent nor significantly different in the “V-light” and “No light” groups on the RGD-bearing microgels in the

deswelling state with low RGD availability. Following quantitative analysis of the immunofluorescence images revealed a significantly higher adhered macrophage number and larger macrophage area in the “N-light” group than in the “V-light” and “No light” groups (Figure S14b, Supporting Information). These results suggest that lateral microgel swelling and deswelling mediate high and low RGD availability, respectively, via expanded and contracted microgel network, which effectively modulated integrin-RGD-binding-mediated macrophage adhesion. When the UCNP, the UCNP shell coating on the UCNP (C), V-light-absorbing natural dye coating, or RGD coating were absent in our material system [RGD-bearing microgels attached to the UCNP (C@S@D)-coated substrate], our N- or V-light-mediated control of macrophage adhesion was not effective (Figures S15a,b, S16a,b, S17a,b, and S18a,b, Supporting Information). This suggests that the necessity of the UCNP (C@S@D) (that can induce swelling of the RGD-bearing microgels) and RGD-specificity for efficient macrophage regulation. These results acquired via utilizing N- and V-light-based system are apparently different from those in previous reports on modulating irreversible RGD uncaging by light^[42,49] or molecular conversion using high-intensity light.^[50]

After confirming the influence of the N-light-mediated swelling and V-light-mediated deswelling of RGD-bearing microgels on macrophage adhesion, we explored the effect of in situ time-regulated light switching on macrophage adhesion. Macrophages on the RGD-bearing microgels attached to the UCNP (C@S@D)-coated substrate were repeatedly or alternately illuminated with N- or V-light at 0, 12, and 24 h (“N-N”, “N-V”, “V-N”, and “V-V” groups) and examined via confocal immunofluorescence imaging and quantifications at 36 h after inducing sufficient macrophage adhesion and polarization.^[19,63–66] For quantifications using fluorescent images, the adhered macrophage numbers were calculated using DAPI-positive macrophage nuclei whereas the adhered macrophage area and elongation factor (the ratio of the major axis to the minor axis) were calculated by using F-actin-stained images of macrophages. We found that the “N-N” group exhibited markedly higher macrophage adhesion compared to the “V-V” group (Figures S19a,b and S20, Supporting Information). Interestingly, in the “V-N” group, macrophage adhesion that was inferior at 12 h (after being subjected to V-mediated RGD-bearing microgels deswelling) was markedly enhanced at 36 h (after being subjected to N-mediated RGD-bearing microgels swelling). Strikingly, in the “N-V” group, macrophage adhesion that was promoted at 12 h (after being subjected to N-mediated RGD-bearing microgels swelling) was suppressed at 36 h (after being subjected to V-light-mediated RGD-bearing microgels deswelling). These results suggest that lateral swelling and deswelling of RGD-bearing microgels lead to high and low RGD availability, respectively, and thus regulated the lateral movement of integrin nanoclusters to modulate integrin-RGD-binding-mediated macrophage adhesion (Scheme 1). We believe that the marked effectiveness of our light-controlled switching system toward time-regulated macrophage adhesion is attributed to the long-term (24 h) stability of the *cis*-state Azobenzene⁺ induced by U-light illumination (Figure 1d,e).

2.4. Light with Different Wavelength Temporally Regulates Macrophage Phenotype

We next examined the effect of in situ temporal light switching on adhesion-dependent macrophage phenotype by using identical light stimulation conditions with either pro-inflammatory (M1) or pro-regenerative (M2) medium. Robust macrophage adhesion including pronounced assembly of cytoskeletal F-actin filaments and adhesion complexes in an elongated shape activates rho-associated protein kinase (ROCK) that stimulates them to acquire pro-regenerative/anti-inflammatory phenotypes.^[18,19] In contrast, macrophages exhibiting poor construction of those adhesion structures in a round shape acquire inflammatory phenotype. Therefore, the effect of in situ temporal light switching on macrophage polarization was investigated by using identical experimental conditions with either inflammatory or regenerative medium. First, we assessed the level of secreted cytokines (IL-4 and IL-10 as M2 markers and TNF- α as a M1 marker) from macrophages cultured on the RGD-bearing microgel-attached UCNP (C@S@D)-coated substrate under N- and V-light irradiation via enzyme-linked immunosorbent assay (ELISA). We found that the “N-N” and “V-N” groups facilitated the release of M2 polarization-related cytokines while they inhibited the release of M1 polarization-related cytokines (Figure 4a,b; Figure S21, Supporting Information). On the other hand, the “V-V” and “N-V” groups stimulated the release of M1 polarization-related cytokine and suppressed the release of M2 polarization-related cytokines. They suggest that the “N-N” and “V-N” groups would highly stimulate M2 polarization of macrophages whereas the “V-V” and “N-V” groups facilitate their M1 polarization.

Confocal immunofluorescence and western blotting imaging of macrophages cultured in either inflammatory or regenerative medium consistently demonstrated that the groups subjected to N-light illumination at later time point (“N-N” and “V-N” groups) predominantly exhibited pro-regenerative/anti-inflammatory phenotypes (low inflammatory iNOS expression when cultured in inflammatory medium and high pro-regenerative/anti-inflammatory Arg-1 expression only when cultured in regenerative medium) regardless of whether using N- or V-light at earlier time point (Figure 4a,b; Figure S22a,b, Supporting Information). Conversely, the groups subjected to V-light illumination at later time point (the “V-V” and “N-V” groups) showed highly inflammatory phenotypes. These findings prove temporal light switchability of macrophage phenotypes via the adhesion structure assembly-mediated pro-regenerative/anti-inflammatory polarization.

We next considered which molecular machinery in the adhesion complexes is involved in the light-mediated temporal regulation of macrophage adhesion that modulates the macrophage phenotypes. We found that the “N-N” and “V-N” groups involving the N-light treatment-mediated swelling of RGD-bearing microgels at later time point effectively stimulated ROCK2 expression regardless of whether using inflammatory or regenerative medium (Figure S23a,b, Supporting Information). The correlation between macrophage adhesion and the inflammatory/regenerative polarization was explored in detail by using

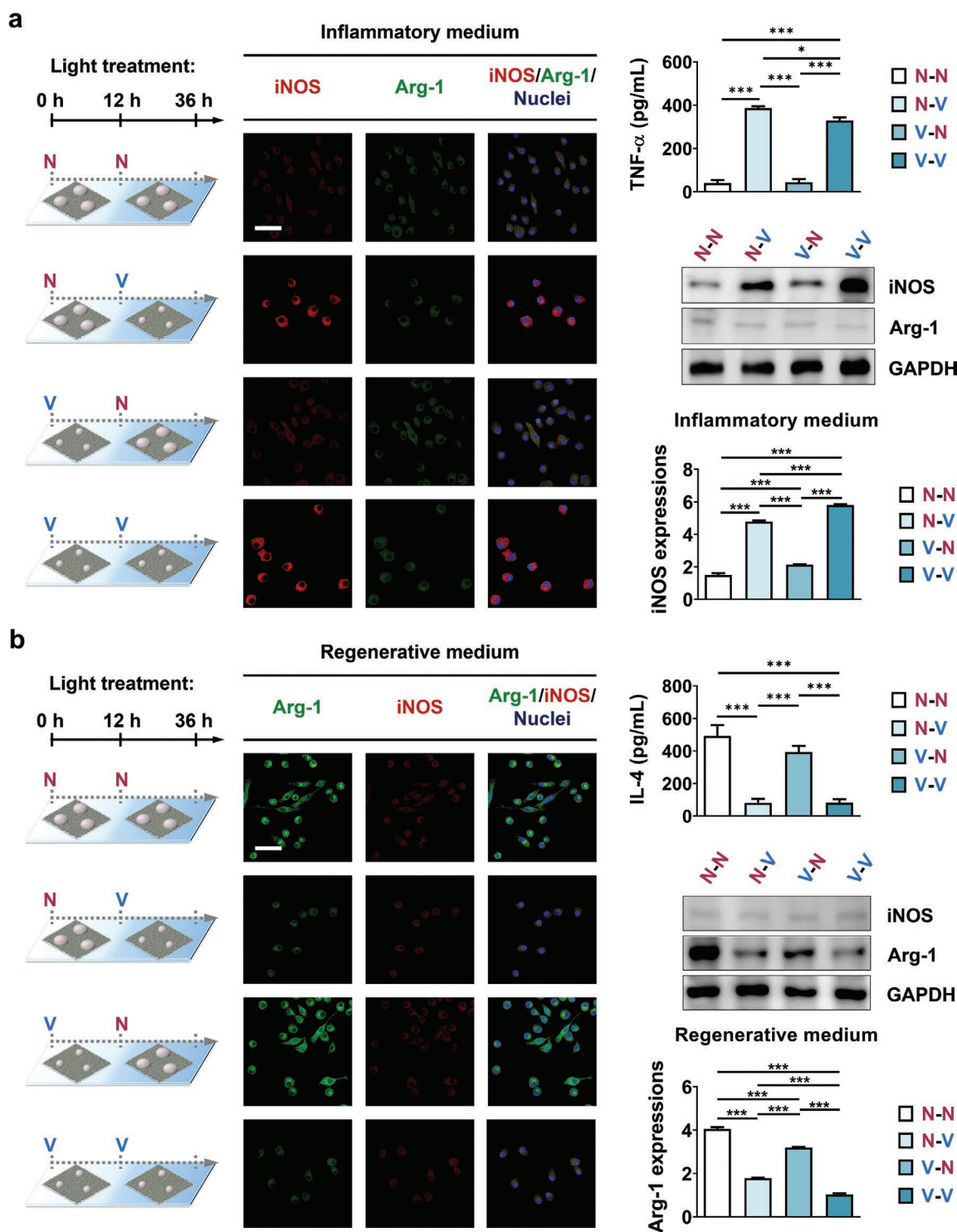


Figure 4. N-light-assisted swelling of RGD-bearing microgels temporally promotes the anti-inflammatory functionality of macrophages. a) Confocal immunofluorescence images of macrophages stained for pro-inflammatory iNOS and pro-regenerative Arg-1 along with nuclei along with quantifications of iNOS protein expression levels (after normalization to that of GAPDH) from western blotting images of adhered macrophages after culturing for 36 h (plated only at 0 h) on the RGD-bearing microgels attached to the UCNP (C@S@D)-coated substrate in pro-inflammatory medium. Secreted TNF- α level of macrophages analyzed by ELISA is also included. At every 12 h after culturing, the substrates in the “N-N”, “N-V”, “V-N”, and “V-V” groups were repeatedly or alternately irradiated with N-light (980 nm at 1 W cm⁻² for 1 min) or V-light (448 nm at 0.2 W cm⁻² for 10 min). b) Confocal immunofluorescence images of macrophages stained for pro-inflammatory iNOS and pro-regenerative Arg-1 along with nuclei and calculations of Arg-1 protein expression levels (after normalization to that of GAPDH) using western blotting images of the adhered macrophages after culturing for 36 h on an identical substrate to that used in (A) in pro-regenerative medium. Secreted IL-4 level of macrophages analyzed by ELISA is also included. Scale bars: 20 μ m. Data are displayed as the mean \pm standard error ($n = 3$). Asterisks were assigned to p values with statistically significant significances (***: $p < 0.001$).

pharmacological inhibitors specific for ROCK, actin polymerization, and myosin II. The inhibition of these consistently repressed macrophage adhesion in terms of spread area and elongated shape irrespective of whether using inflammatory or regenerative medium (Figures S24a,b and S25a,b, Supporting Information). Concomitantly, highly expressed regenerative Arg-1 expression in the “N-N” and “V-N” groups was significantly hindered along with macrophage adhesion repression (by inhibition of ROCK, actin polymerization, or myosin II) in regenerative medium (Figure S24a,b, Supporting Information). Furthermore, highly suppressed expression of inflammatory iNOS in the “N-N” and “V-N” groups cultured in inflammatory medium was found to be negated when ROCK, actin polymerization, or myosin II was inhibited (Figure S25a,b, Supporting Information). These findings collectively confirm that ROCK, actin polymerization, and myosin II are part of the molecular machinery for stimulating adhesion structure formation linked with regenerative M2 polarization and suppressing inflammatory M1 polarization in the “N-N” and “V-N” groups subjected to N-light illumination at later time point.

2.5. N-Light-Mediated Temporal Control of IL-4 Delivery

Since the RGD-bearing microgels differentially respond N- and V-light illumination that induces their swelling and deswelling, respectively, we probed the applicability of these microgels as delivery vehicles for large macromolecules, such as IL-4 with their release controlled by the N- and V-light irradiation (Figure 5a; Figure S26, Supporting Information). Similar to the encapsulation process of fluorescent molecule (rhodamine) into the RGD-bearing microgels, IL-4^[67] may be loaded into the microgels during the cooperative self-assembly of the Azo-C₁₀-N⁺ molecules and the RGD-bearing PAA polymers. We found that the deswelling of the RGD-bearing microgels after V-light treatment for 1 min at 0 and 30 min helped retain the loaded IL-4 for 60 min. In stark contrast, the swelling of the RGD-bearing microgels after U-light treatment for 1 min at 60 and 90 min markedly facilitated the release of the loaded IL-4 for 120 min (Figure 5b). These results prove the swelling-specific time-regulated IL-4 release using our microgel system.

This suggests that the V-light restraining the swelling of the RGD-bearing microgels may retain the loaded IL-4 within the microgels whereas N-light induces the swelling of the RGD-bearing microgels via the H₂O uptake, thereby providing an ample space for the release of loaded IL-4. During the loading of IL-4 proteins into the microgel,^[67] Azo-C₁₀-N⁺ molecules and PAA may physically entrap the IL-4 during microgel network formation of the microgel regardless of its surface charge.^[68,69] When the microgel is in swelling state under U-light illumination, the expanded microgel space untraps the IL-4 and stimulates the release via the widen free space. Under V-light illumination, the microgel space is contracted and IL-4 remains entrapped within the microgel. Furthermore, our microgels may function as the universal delivery vector for diverse proteins, small molecules, and others.

2.6. Light-Mediated IL-4 Delivery and Temporal Macrophage Regulation In Vivo

The dynamic effect of temporal switching of lateral swelling and deswelling of RGD-bearing microgels on IL-4 release and host cell regulation was investigated via N- and V-light irradiation without using U-light was investigated. Intriguingly, our microgel dynamics emulate tissues and organs, such as lung, heart, and brain, which repeatedly swell and deswell via fluid transfer, thereby dynamically regulating integrin-RGD interactions that occur in the nanoscale structure of biopolymer network.^[70–72] Macrophages are host cells that are dominantly involved in the early host responses that regulate the late responses, such as inflammation and tissue regeneration.^[10–12] To this end, we subcutaneously implanted pro-regenerative IL-4-loaded RGD-bearing microgels attached to the UCNP (C@S@D)-coated substrate that functions as the efficient N-light-to-U-light upconverter in vivo. For brief explanation of practical length scales, we have subcutaneously implanted the UCNP (C@S@D)-coated silicon substrate (12 mm × 12 mm) in the backs of mice within 1 mm tissue depth. For in situ temporal switching of the swelling and deswelling of RGD-bearing microgels, we applied N-light (980 nm at 1 W cm⁻² for 1 min) or V-light (448 nm at 0.2 W cm⁻² for 10 min) at ≈5 cm away from the mice to have uniform laser intensity exerted on the silicon substrate. The implanted materials in the backs of the mice were repeatedly or alternately irradiated with external N- or V-light at 0 and 12 h after implantation to facilitate in situ swelling and deswelling of RGD-bearing microgels. Host macrophages adhered onto the implants were analyzed at 24 h after implantation. In vivo stability of RGD-bearing microgels was examined via confocal imaging of the rhodamine-encapsulated RGD-bearing microgels on the UCNP (C@S@D)-coated substrate before and after implantation. We found that the similar number of red-fluorescent RGD-bearing microgels was uniformly distributed, thereby confirming the excellent stability of our materials in vivo (Figure 5c,d).

We analyzed host macrophages via confocal immunofluorescence imaging of host cells expressing either inflammatory (iNOS and CD86) and regenerative (Arg-1 and STAB1) macrophage markers. We found that both the “N-N” and “V-N” groups with high swelling-mediated elevation of RGD availability exhibited pronouncedly higher adhered cell numbers with larger spread areas and elongation factors of host macrophages^[73] than the “N-V” and “V-V” groups exhibiting low deswelling-mediated suppression of RGD availability (Figure 5e; Figures S27a,c, S28a,b, and S29a,b, Supporting Information). In the “N-N” and “V-N” groups that promote the swelling-facilitated IL-4 release, Arg-1 and STAB1 expressions were highly stimulated while iNOS and CD86 expression were markedly suppressed compared with the “N-V” and “V-V” groups. Taken together, we believe that the pro-regenerative polarization of host macrophages in the “N-N” and “V-N” groups was highly stimulated in response to the synergistic effect of intensified adhesion to the highly available RGDs and facilitated pro-regenerative IL-4 release. Furthermore, host macrophages

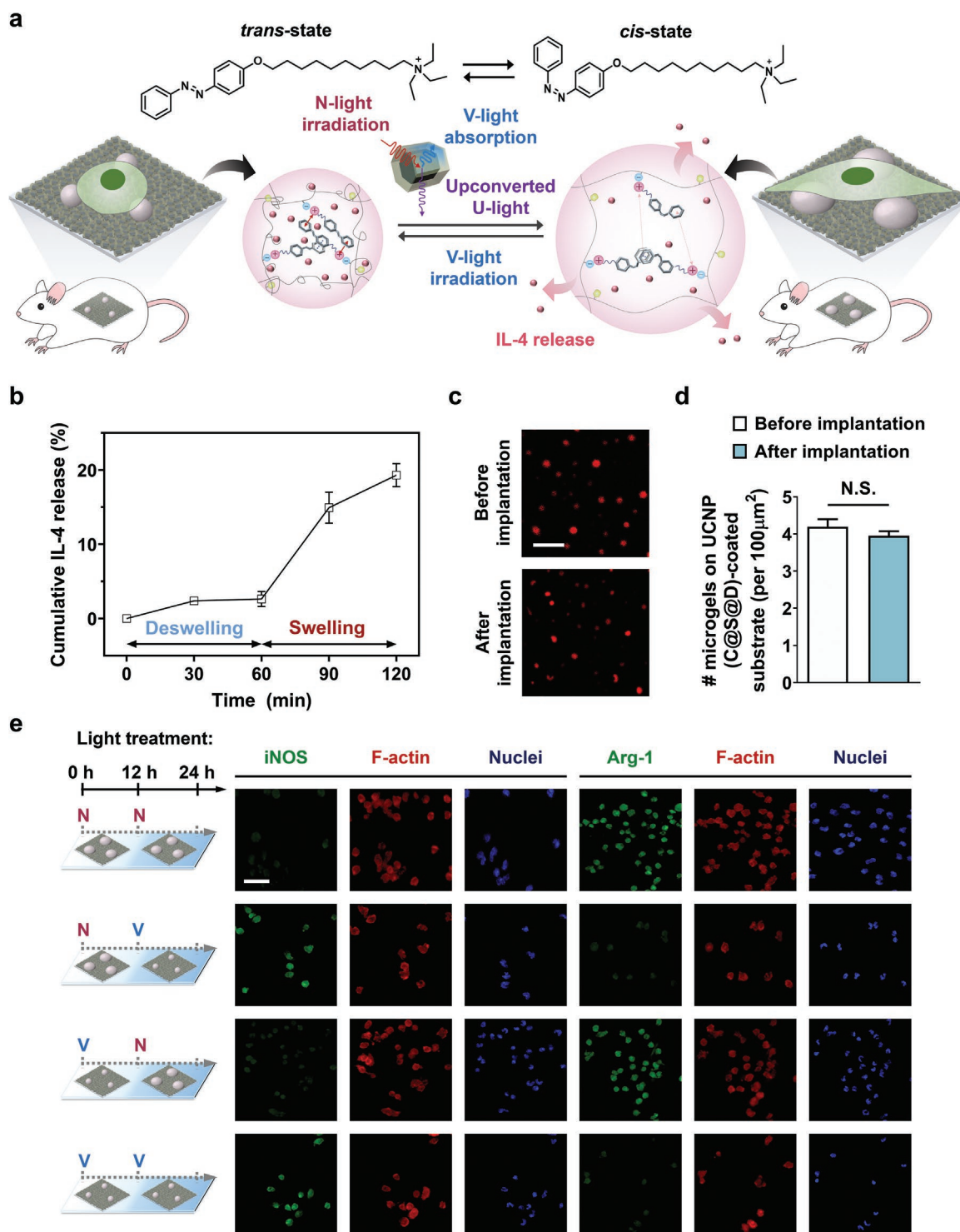


Figure 5. Remote switching of the swelling of RGD-bearing microgels via tissue-penetrative light enables time-regulated IL-4 delivery and host cell regulation in vivo. a) A schematic of N-light-upconverted U-light mediating the swelling of subcutaneously implanted RGD-bearing microgels, thereby triggering the diffusional release of interleukin-4 (IL-4) for host cell regulation. b) The percentage of cumulative IL-4 release of RGD-bearing microgels by V-light treatment for 1 min each at 0 and 30 min followed by U-light treatment for 1 min each at 60 and 90 min. c) Confocal fluorescence images of rhodamine-loaded RGD-bearing microgels attached to the UCNP (C@S@D)-coated substrate and d) computations of the density of rhodamine-fluorescent RGD-bearing microgels on the substrate before and after subcutaneous implantation. e) Confocal immunofluorescence images of iNOS and Arg-1 along with F-actin, and nuclei of recruited host cells onto the RGD-bearing microgels attached to the UCNP (C@S@D)-coated substrate at 24 h after subcutaneous implantation. At 0 and 12 h after implantation, the backs of the mice (toward the substrate) in the “N-N”, “N-V”, “V-N”, and “V-V” groups were repeatedly or alternately externally illuminated with N-light (980 nm at 1 W cm⁻² for 1 min) or V-light (448 nm at 0.2 W cm⁻² for 10 min). Scale bars: (c) 10 and (e) 20 μm. Data are shown as the mean ± standard error (*n* = 10). N.S. indicates non-statistically significant differences.

(which are typically recruited 12 h after implantation) in the “V-N” group showed enhanced regenerative phenotypes after 12 h than those in the “N-V” group after 0 h due to longer exposure to the N-light-triggered IL-4 release. Although we focused on analyzing host macrophage regulation, NIMP-R14-positive host neutrophils were also recruited to the implanted materials during the early host responses within 24 h after implantation (Figure S30a,b, Supporting Information).

It has been previously reported that UCNPs coated with PAA^[74] or coupled with azobenzene^[75] are not toxic even for long-term period over 4 months, and consequently, the UCNP-based materials have been undergoing clinical trials.^[76,77] In accordance with these previous reports, we found that the RGD-bearing microgels on the UCNP (C@S@D)-coated substrate subjected to the N- and V-light irradiation without using U-light are not toxic to both subcutaneous tissue (localized) and various organs (systemic), such as liver, kidney, spleen, and heart, as evidenced by no differences in the cell structure before and 7 days after implantation and treatment with N- or V-light irradiation (Figure S31, Supporting Information). Our tissue-penetrative stimuli-mediated controllable system is evidently different from previous *in vivo* studies utilizing highly tissue-absorptive and harmful U-light to “irreversibly” trigger RGD uncaging or N-light to “irreversibly” cleave caging molecules to trigger the release of drug molecules *in vivo*.^[49] Our remote and safe system without using U-light offers temporal controllability toward macromolecule delivery and *in vivo* host cell regulation.

3. Conclusion

We have harnessed self-assembly of Azo-C₁₀-N⁺ molecules via intermolecular interactions that incorporate RGD-bearing anionic polymers via electrostatic interactions. Tissue-penetrative N-light treatment mediated preferential N-light-to-U-light transduction by using UCNP (C@S@D) induced hydrophilic *cis*-state formation of Azo-C₁₀-N⁺ molecules with suppressed π -cation interactions in loosely packed structures, as verified via MD simulations. This induced the lateral swelling exhibiting highly available RGDs via RGD-bearing polymer uncoiling that facilitates macrophage adhesion structure formation and IL-4 release for promoting pro-regenerative polarization. V-light treatment induced the hydrophobic *trans*-state formation of Azo-C₁₀-N⁺ molecules with enhanced π -cation interactions in densely packed structures that facilitated lateral deswelling (as verified by *in situ* real-time confocal microscopy imaging), which restrained RGD availability via RGD-bearing polymer coiling, thereby inhibiting macrophage adhesion. Versatile tuning of azobenzene derivatives can offer unlimited tunability of redshifting V-light wavelength to further enhance tissue-penetrative capability and lifetime of the *cis*-state.^[43] RGD-bearing microgels can be diversified with the use of various ligands and protein delivery that can be used to regulate a myriad of host cells. Also, upon the swelling and deswelling, microgels can uptake and release body fluids for diagnosis analysis. Our light controllable system can also be utilized as solar thermal fuels that can capture, convert, and release solar energy via photoisomerization-regulated self-assembly.^[33]

Supporting Information

Supporting Information is available from the Wiley Online Library or from the author.

Acknowledgements

This work was supported by the National Research Foundation of Korea (NRF) grant funded by the Korean government (MSIT) (No. 2020R1C1C1011038, 2021R1A2C2005418, 2022M3H4A1A03076638, and 2022R1A2C2005943). This work was also supported by a Korea University Grant and the KIST intramural program. HAADF-STEM was conducted with the support of the Seoul Center in Korea Basic Science Institute (KBSI). Animal experiments in this study were conducted after an approval from the Institutional Animal Care and Use Committee at Korea University (KOREA-2021-0006).

Note: The formatting of the text Azo-C₁₀-N⁺ in Section 2.1 (page 4 right column), 3 places, and Section 2.5 (page 11, left column), 1 place, was corrected after initial publication online.

Conflict of Interest

The authors declare no conflict of interest.

Data Availability Statement

The data that support the findings of this study are available from the corresponding author upon reasonable request.

Keywords

dynamic hydrogels, macrophage adhesion, macrophage polarization, microgel swelling, photoswitchable microgels

Received: June 16, 2022
Revised: September 22, 2022
Published online:

- [1] A. S. Tayi, A. K. Shveyd, A. C.-H. Sue, J. M. Szarko, B. S. Rolczynski, D. Cao, T. J. Kennedy, A. A. Sarjeant, C. L. Stern, W. F. Paxton, W. Wu, S. K. Dey, A. C. Fahrenbach, J. R. Guest, H. Mohseni, L. X. Chen, K. L. Wang, J. F. Stoddart, S. I. Stupp, *Nature* **2012**, 488, 485.
- [2] Z. L. Yu, F. Tantakitti, T. Yu, L. C. Palmer, G. C. Schatz, S. I. Stupp, *Science* **2016**, 351, 497.
- [3] D. P. August, R. A. W. Dryfe, S. J. Haigh, P. R. C. Kent, D. A. Leigh, J.-F. Lemonnier, Z. Li, C. A. Muryn, L. I. Palmer, Y. Song, G. F. S. Whitehead, R. J. Young, *Nature* **2020**, 588, 429.
- [4] B. Sun, Y. Kim, Y. Wang, H. Wang, J. Kim, X. Liu, M. Lee, *Nat. Mater.* **2018**, 17, 599.
- [5] W. Baek, M. S. Bootharaju, K. M. Walsh, S. Lee, D. R. Gamelin, T. Hyeon, *Nat. Mater.* **2021**, 20, 650.
- [6] W. Jiang, Z. Qu, P. Kumar, D. Vecchio, Y. Wang, Y. Ma, J. H. Bahng, K. Bernardino, W. R. Gomes, F. M. Colombari, A. Lozada-Blanco, M. Veksler, E. Marino, A. Simon, C. Murray, S. R. Muniz, A. F. de Moura, N. A. Kotov, *Science* **2020**, 368, 642.
- [7] Y. Li, M. Zhou, Y. Song, T. Higaki, H. Wang, R. Jin, *Nature* **2021**, 594, 380.
- [8] G. A. Hudalla, T. Sun, J. Z. Gasiorowski, H. Han, Y. F. Tian, A. S. Chong, J. H. Collier, *Nat. Mater.* **2014**, 13, 829.

- [9] J. Liu, Y. S. Kim, C. E. Richardson, A. Tom, C. Ramakrishnan, F. Birey, T. Katsumata, S. C. Chen, C. Wang, X. Wang, L.-M. Joubert, Y. Jiang, H. Wang, L. E. Fenno, J. B.-H. Tok, S. P. Pasca, K. Shen, Z. Bao, K. Deisseroth, *Science* **2020**, *367*, 1372.
- [10] K. Sadtler, A. Singh, M. T. Wolf, X. Wang, D. M. Pardoll, J. H. Elisseeff, *Nat. Rev. Mater.* **2016**, *1*, 16040.
- [11] O. Veisoh, J. C. Doloff, M. Ma, A. J. Vegas, H. H. Tam, A. R. Bader, J. Li, E. Langan, J. Wyckoff, W. S. Loo, S. Jhunjunwala, A. Chiu, S. Siebert, K. Tang, J. Hollister-Lock, S. Aresta-Dasilva, M. Bochenek, J. Mendoza-Elias, Y. Wang, M. Qi, D. M. Lavin, M. Chen, N. Dholakia, R. Thakrar, I. Lacik, G. C. Weir, J. Oberholzer, D. L. Greiner, R. Langer, D. G. Anderson, *Nat. Mater.* **2015**, *14*, 643.
- [12] J. Han, Y. S. Kim, M.-Y. Lim, H. Y. Kim, S. Kong, M. Kang, Y. W. Choo, J. H. Jun, S. Ryu, H.-Y. Jeong, J. Park, G.-J. Jeong, J.-C. Lee, G. H. Eom, Y. Ahn, B.-S. Kim, *ACS Nano* **2018**, *12*, 1959.
- [13] J. Li, X. Jiang, H. Li, M. Gelinsky, Z. Gu, *Adv. Mater.* **2021**, *33*, 2004172.
- [14] J. Fu, Y. Li, Y. Zhang, Y. Liang, Y. Zheng, Z. Li, S. Zhu, C. Li, Z. Cui, S. Wu, *Adv. Mater.* **2021**, *33*, 2102926.
- [15] Y. Wang, J. Yu, Z. Luo, Q. Shi, G. Liu, F. Wu, Z. Wang, Y. Huang, D. Zhou, *Adv. Mater.* **2021**, *33*, 2103497.
- [16] C. Cai, X. Zhang, Y. Li, X. Liu, S. Wang, M. Lu, X. Yan, L. Deng, S. Liu, F. Wang, C. Fan, *Adv. Mater.* **2021**, *34*, 2106564.
- [17] N. Qiu, G. Wang, J. Wang, Q. Zhou, M. Guo, Y. Wang, X. Hu, H. Zhou, R. Bai, M. You, Z. Zhang, C. Chen, Y. Liu, Y. Shen, *Adv. Mater.* **2021**, *33*, 2006189.
- [18] S. Zandi, S. Nakao, K.-H. Chun, P. Fiorina, D. Sun, R. Arita, M. Zhao, E. Kim, O. Schueller, S. Campbell, M. Taher, M. I. Melhorn, A. Schering, F. Gatti, S. Tezza, F. Xie, A. Vergani, S. Yoshida, K. Ishikawa, M. Yamaguchi, F. Sasaki, R. Schmidt-Ullrich, Y. Hata, H. Enaida, M. Yuzawa, T. Yokomizo, Y.-B. Kim, P. Sweetnam, T. Ishibashi, A. Hafezi-Moghadam, *Cell Rep.* **2015**, *10*, 1173.
- [19] F. Y. McWhorter, T. Wang, P. Nguyen, T. Chung, W. F. Liu, *Proc. Natl. Acad. Sci. USA* **2013**, *110*, 17253.
- [20] L. Sun, F. Shen, L. Tian, H. Tao, Z. Xiong, J. Xu, Z. Liu, *Adv. Mater.* **2021**, *33*, 2007910.
- [21] H. Jeong, W. Park, D.-H. Kim, K. Na, *Adv. Drug Deliv. Rev.* **2021**, *177*, 113954.
- [22] N. Kim, E. Kim, H. Kim, M. R. Thomas, A. Najer, M. M. Stevens, *Adv. Mater.* **2021**, *33*, 2007738.
- [23] A. Bédier, F. Bonini, C. A. Verheyen, M. Genta, M. Martins, J. Brefie-Guth, J. Tratwal, A. Filippova, P. Burch, O. Naveiras, T. Braschler, *Adv. Mater.* **2021**, *33*, 2102350.
- [24] Y. Zou, B. Huang, L. Cao, Y. Deng, J. Su, *Adv. Mater.* **2021**, *33*, 2005215.
- [25] Y. Zhu, S. Li, J. Li, N. Falcone, Q. Cui, S. Shah, M. C. Hartel, N. Yu, P. Young, N. R. de Barros, Z. Wu, M. Ermis, R. Haghniaz, C. Wang, H. Kang, J. Lee, S. Karamikamkar, S. Ahadian, V. Jucaud, M. R. Dokmeci, H.-J. Kim, A. Khademhosseini, *Adv. Mater.* **2022**, *34*, 2108389.
- [26] M. Ryma, T. Tylek, J. Liebscher, C. Blum, R. Fernandez, C. Böhm, W. Kastenmüller, G. Gasteiger, J. Groll, *Adv. Mater.* **2021**, *33*, 2101228.
- [27] S. Li, X. Guo, R. Gao, M. Sun, L. Xu, C. Xu, H. Kuang, *Adv. Mater.* **2021**, *33*, 2005424.
- [28] S. Vermeulen, F. Honig, A. Vasilevich, N. Roumans, M. Romero, A. D. Eren, U. Tuvshindorj, M. Alexander, A. Carlier, P. Williams, J. Uquillas, J. de Boer, *Adv. Mater.* **2021**, *33*, 2102084.
- [29] C. F. Guimarães, A. P. Marques, R. L. Reis, *Adv. Mater.* **2022**, *34*, 2105645.
- [30] Y. Kim, H. Choi, J. E. Shin, G. Bae, R. Thangam, H. Kang, *View* **2020**, *1*, 20200029.
- [31] A. M. Rosales, K. S. Anseth, *Nat. Rev. Mater.* **2016**, *1*, 15012.
- [32] C. Gong, S. Sun, Y. Zhang, L. Sun, Z. Su, A. Wu, G. Wei, *Nanoscale* **2019**, *11*, 4147.
- [33] L. Dong, Y. Feng, L. Wang, W. Feng, *Chem. Soc. Rev.* **2018**, *47*, 7339.
- [34] A. Zakharchenko, N. Guz, A. M. Laradji, E. Katz, S. Minko, *Nat. Catal.* **2018**, *1*, 73.
- [35] J.-u. Lee, W. Shin, Y. Lim, J. Kim, W. R. Kim, H. Kim, J.-H. Lee, J. Cheon, *Nat. Mater.* **2021**, *20*, 1029.
- [36] S. Min, M. J. Ko, H. J. Jung, W. Kim, S.-B. Han, Y. Kim, G. Bae, S. Lee, R. Thangam, H. Choi, N. Li, J. E. Shin, Y. S. Jeon, H. S. Park, Y. J. Kim, U. K. Sukumar, J.-J. Song, S.-K. Park, S.-H. Yu, Y. C. Kang, K.-B. Lee, Q. Wei, D.-H. Kim, S. M. Han, R. Paulmurugan, Y. K. Kim, H. Kang, *Adv. Mater.* **2021**, *33*, 2008353.
- [37] G. Bae, M. S. Kim, R. Thangam, T. M. Koo, W. Y. Jang, J. Yoon, S.-B. Han, L. Yang, S. Y. Kim, N. Kang, S. Min, H. Hong, H. E. Fu, M. J. Ko, D.-H. Kim, W. K. Jeong, D.-H. Kim, T.-H. Kim, J.-W. Choi, K.-B. Lee, R. Paulmurugan, Y. Zhu, H.-J. Kim, J. Lee, J. S. Kim, A. Khademhosseini, Y. K. Kim, H. Kang, *Adv. Funct. Mater.* **2022**, *32*, 2200828.
- [38] S. Min, Y. S. Jeon, H. J. Jung, C. Khatua, N. Li, G. Bae, H. Choi, H. Hong, J. E. Shin, M. J. Ko, H. S. Ko, I. Jun, H. E. Fu, S. H. Kim, R. Thangam, J. J. Song, V. P. Dravid, Y. K. Kim, H. Kang, *Adv. Mater.* **2020**, *32*, 2004300.
- [39] A. Cheesbrough, F. Sciscione, F. Riccio, P. Harley, L. R'Bibo, G. Ziakas, A. Darbyshire, I. Lieberam, W. Song, *Adv. Mater.* **2022**, *34*, 2110441.
- [40] J. Wang, Y. Liu, M. Morsch, Y. Lu, P. Shangguan, L. Han, Z. Wang, X. Chen, C. Song, S. Liu, B. Shi, B. Z. Tang, *Adv. Mater.* **2022**, *34*, 2106082.
- [41] Y. Ding, Z. Tong, L. Jin, B. Ye, J. Zhou, Z. Sun, H. Yang, L. Hong, F. Huang, W. Wang, Z. Mao, *Adv. Mater.* **2022**, *34*, 2106388.
- [42] T. T. Lee, J. R. Garcia, J. I. Paez, A. Singh, E. A. Phelps, S. Weis, Z. Shafiq, A. Shekaran, A. del Campo, A. J. Garcia, *Nat. Mater.* **2015**, *14*, 352.
- [43] A. A. Beharry, G. A. Woolley, *Chem. Soc. Rev.* **2011**, *40*, 4422.
- [44] Y. Chen, Z. Wang, Y. He, Y. J. Yoon, J. Jung, G. Zhang, Z. Lin, *Proc. Natl. Acad. Sci. USA* **2018**, *115*, E1391.
- [45] Y. Cai, Z. Guo, J. Chen, W. Li, L. Zhong, Y. Gao, L. Jiang, L. Chi, H. Tian, W.-H. Zhu, *J. Am. Chem. Soc.* **2016**, *138*, 2219.
- [46] K. Iwaso, Y. Takashima, A. Harada, *Nat. Chem.* **2016**, *8*, 625.
- [47] B. Adhikari, Y. Yamada, M. Yamauchi, K. Wakita, X. Lin, K. Aratsu, T. Ohba, T. Karatsu, M. J. Hollamby, N. Shimizu, H. Takagi, R. Haruki, S.-i. Adachi, S. Yagai, *Nat. Commun.* **2017**, *8*, 15254.
- [48] F. Wang, R. Deng, J. Wang, Q. Wang, Y. Han, H. Zhu, X. Chen, X. Liu, *Nat. Mater.* **2011**, *10*, 968.
- [49] H. Kang, K. Zhang, Q. Pan, S. Lin, D. S. H. Wong, J. Li, W. Y.-W. Lee, B. Yang, F. Han, G. Li, B. Li, L. Bian, *Adv. Funct. Mater.* **2018**, *28*, 1802642.
- [50] W. Li, Z. Chen, L. Zhou, Z. Li, J. Ren, X. Qu, *J. Am. Chem. Soc.* **2015**, *137*, 8199.
- [51] W. Li, Z. Yan, J. Ren, X. Qu, *Chem. Soc. Rev.* **2018**, *47*, 8639.
- [52] R. Glazier, J. M. Brockman, E. Bartle, A. L. Mattheyses, O. Destaing, K. Salaita, *Nat. Commun.* **2019**, *10*, 4507.
- [53] J. H. Fendler, *Chem. Mater.* **2001**, *13*, 3196.
- [54] A. K. Gaharwar, I. Singh, A. Khademhosseini, *Nat. Rev. Mater.* **2020**, *5*, 686.
- [55] C. Gao, Y. Wang, Z. Ye, Z. Lin, X. Ma, Q. He, *Adv. Mater.* **2021**, *33*, 2000512.
- [56] P. Arya, J. Jelken, N. Lomadze, S. Santer, M. Bekir, *J. Chem. Phys.* **2020**, *152*, 024904.
- [57] P. Arya, J. Jelken, D. Feldmann, N. Lomadze, S. Santer, *J. Chem. Phys.* **2020**, *152*, 194703.
- [58] Y. Zakrevskyy, J. Roxlau, G. Brezesinski, N. Lomadze, S. Santer, *J. Chem. Phys.* **2014**, *140*, 01B612_1.
- [59] S. Han, R. Deng, X. Xie, X. Liu, *Angew. Chem., Int. Ed.* **2014**, *53*, 11702.
- [60] M. Rafeian-Kopaei, A. Baradaran, M. Rafeian, *J. Nephropathol.* **2013**, *2*, 152.
- [61] J. A. Deeg, I. Louban, D. Aydin, C. Selhuber-Unkel, H. Kessler, J. P. Spatz, *Nano Lett.* **2011**, *11*, 1469.

- [62] X. Wang, S. Li, C. Yan, P. Liu, J. Ding, *Nano Lett.* **2015**, *15*, 1457.
- [63] Y. Zhu, H. Liang, X. Liu, J. Wu, C. Yang, T. M. Wong, K. Y. Kwan, K. M. Cheung, S. Wu, K. W. Yeung, *Sci. Adv.* **2021**, *7*, eabf6654.
- [64] K. Wang, W.-D. Hou, X. Wang, C. Han, I. Vuletic, N. Su, W.-X. Zhang, Q.-S. Ren, L. Chen, Y. Luo, *Biomaterials* **2016**, *102*, 249.
- [65] Y. Kim, H. J. Jung, Y. Lee, S. Koo, R. Thangam, W. Y. Jang, S. Y. Kim, S. Park, S. Lee, G. Bae, K. D. Patel, Q. Wei, K.-B. Lee, R. Paulmurugan, W. K. Jeong, T. Hyeon, D. Kim, H. Kang, *J. Am. Chem. Soc.* **2022**, *144*, 5769.
- [66] Y. Kim, T. M. Koo, R. Thangam, M. S. Kim, W. Y. Jang, N. Kang, S. Min, S. Y. Kim, L. Yang, H. Hong, H. J. Jung, E. K. Koh, K. D. Patel, S. Lee, H. E. Fu, Y. S. Jeon, B. C. Park, S. Y. Kim, S. Park, J. Lee, L. Gu, D.-H. Kim, T.-H. Kim, K.-B. Lee, W. K. Jeong, R. Paulmurugan, Y. K. Kim, H. Kang, *Adv. Mater.* **2022**, *34*, 2110340.
- [67] Y. Wang, B.-J. Shen, W. Sebald, *Proc. Natl. Acad. Sci. USA* **1997**, *94*, 1657.
- [68] C.-C. Lin, A. T. Metters, *Adv. Drug Delivery Rev.* **2006**, *58*, 1379.
- [69] J. T.-W. Wang, A. C. Rodrigo, A. K. Patterson, K. Hawkins, M. M. S. Aly, J. Sun, K. T. Al Jamal, D. K. Smith, *Adv. Sci.* **2021**, *8*, 2101058.
- [70] J. K. Mouw, G. Ou, V. M. Weaver, *Nat. Rev. Mol. Cell Biol.* **2014**, *15*, 771.
- [71] M. Carlsson, P. Cain, C. Holmqvist, F. Stahlberg, S. Lundback, H. Arheden, *Am. J. Physiol.: Heart Circ. Physiol.* **2004**, *287*, H243.
- [72] S. I. Rapoport, M. Hori, I. Klatzo, *Science* **1971**, *173*, 1026.
- [73] C. W. ShieldsIV, M. A. Evans, L. L.-W. Wang, N. Baugh, S. Iyer, D. Wu, Z. Zhao, A. Pusuluri, A. Ukidve, D. C. Pan, *Sci. Adv.* **2020**, *6*, eaaz6579.
- [74] L. Xiong, T. Yang, Y. Yang, C. Xu, F. Li, *Biomaterials* **2010**, *31*, 7078.
- [75] Y. Zhang, Y. Zhang, G. Song, Y. He, X. Zhang, Y. Liu, H. Ju, *Angew. Chem.* **2019**, *131*, 18375.
- [76] H. Oliveira, A. Bednarkiewicz, A. Falk, E. Fröhlich, D. Lisjak, A. Prina-Mello, S. Resch, C. Schimpel, I. V. Vrček, E. Wysokińska, *Adv. Healthcare Mater.* **2019**, *8*, 1801233.
- [77] Z. Hu, W.-H. Chen, J. Tian, Z. Cheng, *Trends Mol. Med.* **2020**, *26*, 469.